December 29, 2019

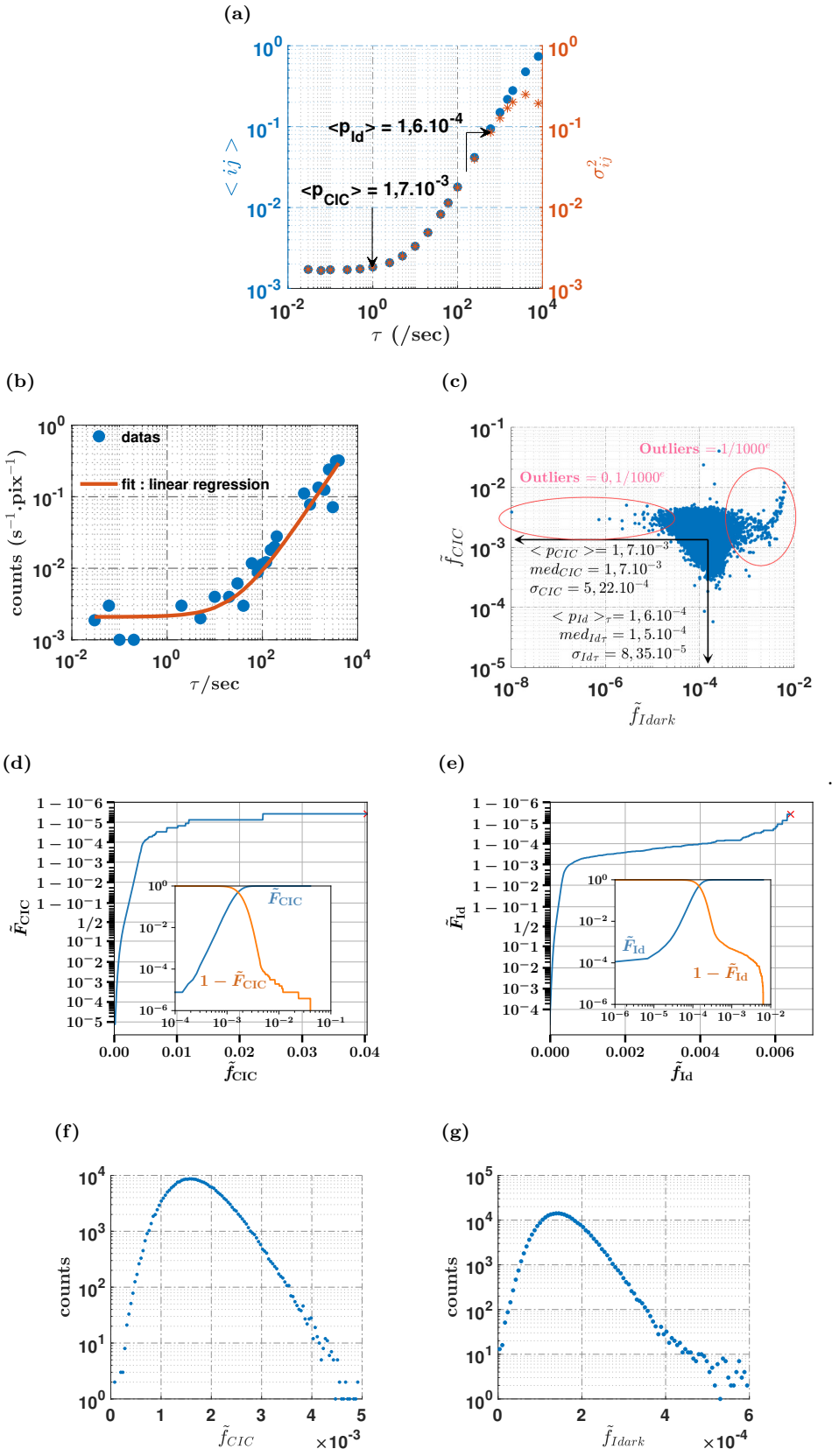

Figure 1 – **Global detector response.** Evolution of the frequency of counts with the time of exposure (a) . **single pixel : exemple of fit.** The individual pixel average noise response to an increased time of exposure τ was extracted and fitted out of saturation by weighted linear regression (b). In those conditions the linear response is considered such as $<\text{pixel}_{ij}>_K = CIC + Id * \tau$. **Caracterisation of single pixel response.** Single pixel response statistics (c). Cumulative distribution (CDF) of the Clock Induced Charges (CIC) noise (d) and the dark current (Id) (e) : Arctanh transform representation with insert in logarithmic scale of the CDF and 1-CDF. Histograms of the CIC (f) and the Id (g).

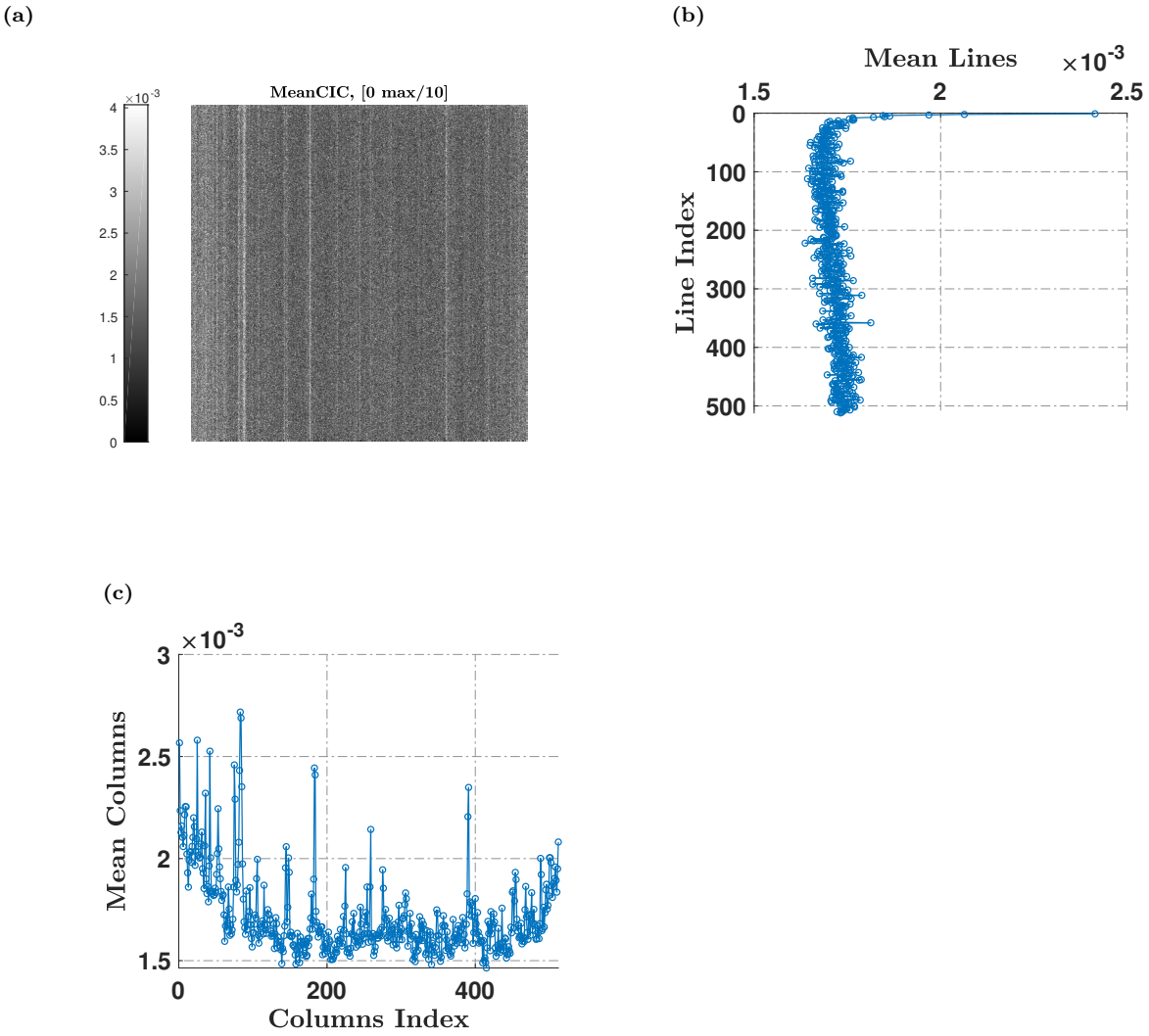

Figure 2 – **Lines and Column Pattern for CIC**. Image of the CIC mean with a maximum threshold set to $1/10^e$ of the maximal pixel value.((a).) Profile of the CIC lines (mean) ((b).) Profile of the CIC columns (mean)((c).)

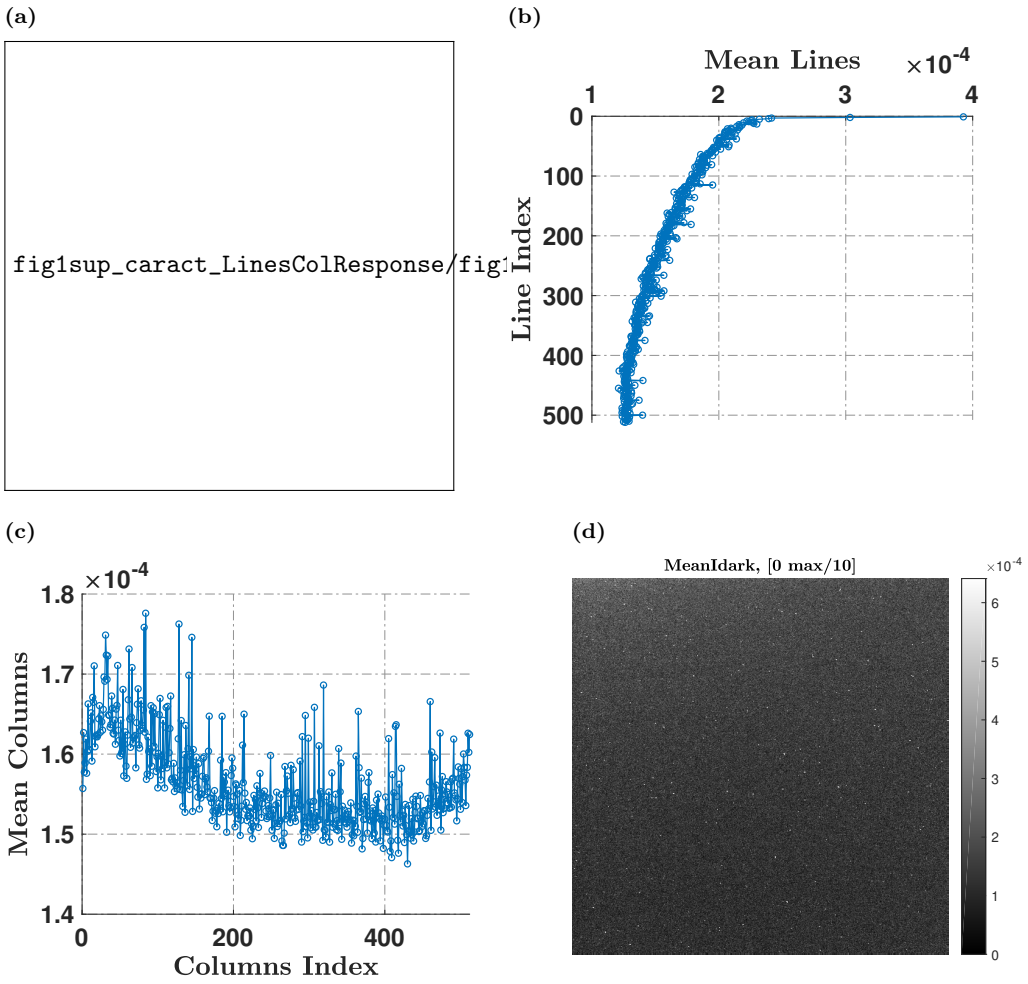

Figure 3 – **Lines and Column Pattern for Id**. Image of the Id mean with a maximum threshold set to $1/40^e$ of the maximal pixel value.((a).) Profile of the Id lines (mean) ((b).) Profile of the Id columns (mean) ((c).) Image of the Id mean with a maximum threshold set to $1/10^e$ of the maximal pixel value.((d).)

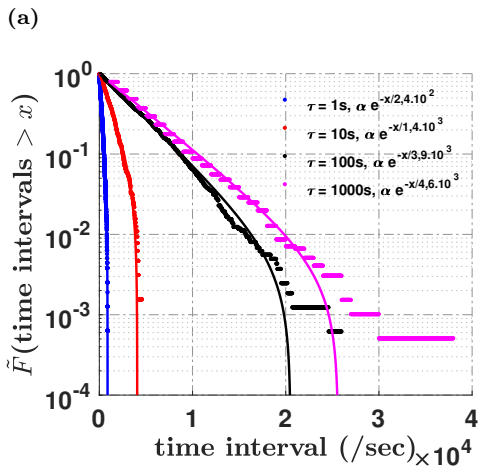

Figure 4 – **Distribution of time intervals.** The complement of the cumulative distribution of the time intervals between two successive counts for a pixel$_{ij}$ for all pixels is represented. The time intervals are exctracted for differents times of exposure τ and fitted by an exponential model. For each τ, the time constant found according to the model is given (a)

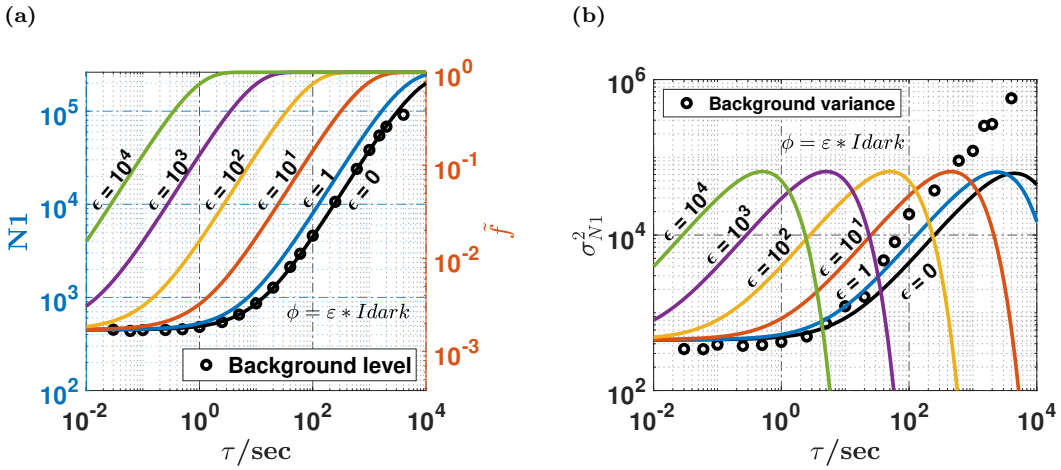

Figure 5 – **wide detector response : simulation and data.** The model gives the simulation of the wide detector response N1 (N1 = $\sum_{ij}$pixels) (a) and its variance (b) for different fluxes. The experimental noise (N1) and its variance are represented.

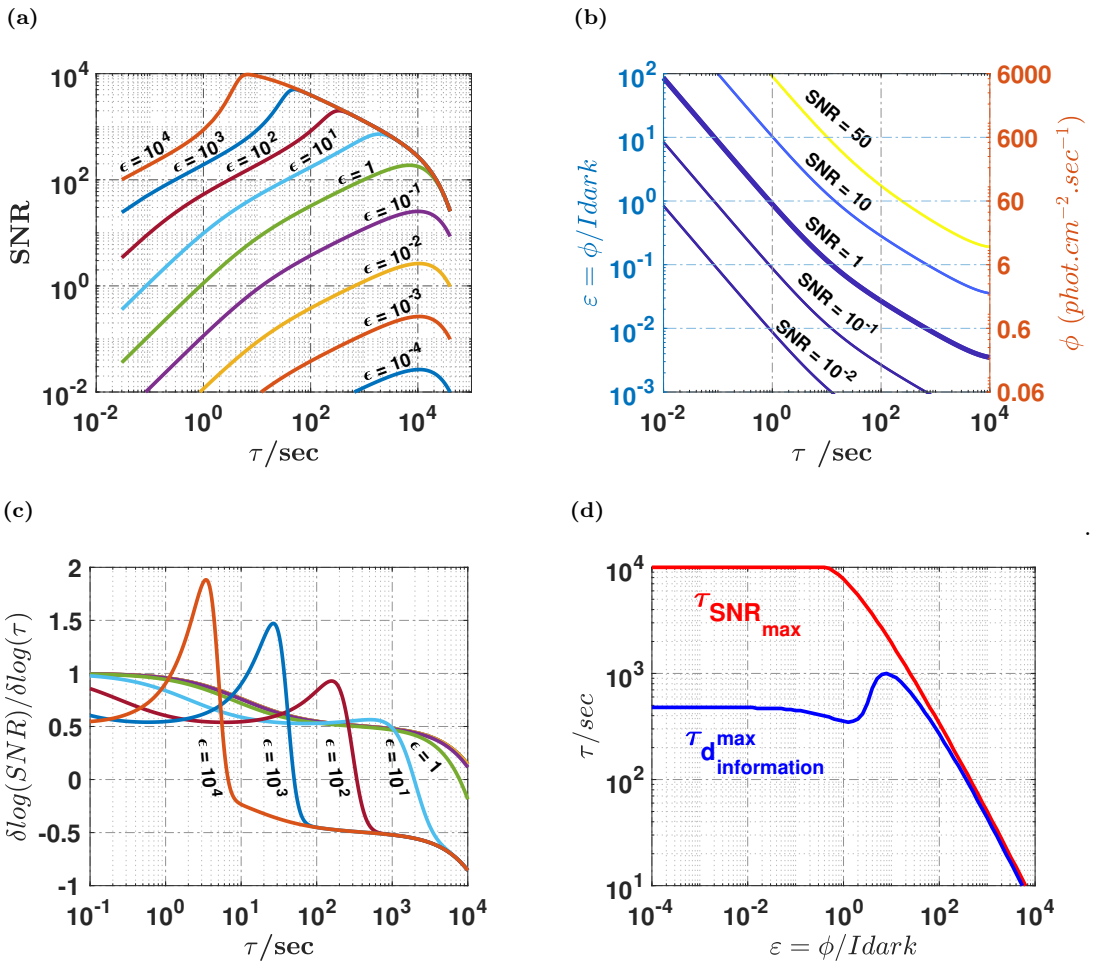

Figure 6 – **SNR simulation.** The SNR simulation is represented for different fluxes ϕ expressed as a fraction ϵ of the dark current Id. The x axes is extended to 10^5 seconds to show the effect of the saturation on the SNR in photon counting mode (a). Figure (b) shows the corresponding SNR contour plot. **What is the optimal time of exposure.** Figure (c) shows the logarithmic derivative of the SNR ($\delta logSNR/\delta log\tau$) for different fluxes. The time of maximal information density ($\tau_{d^{max}_{info}}$) is such as $\delta logSNR/\delta log\tau = 0,5$ (d). The time of maximal SNR ($\tau_{SNR^{max}}$) is comparatively represented.

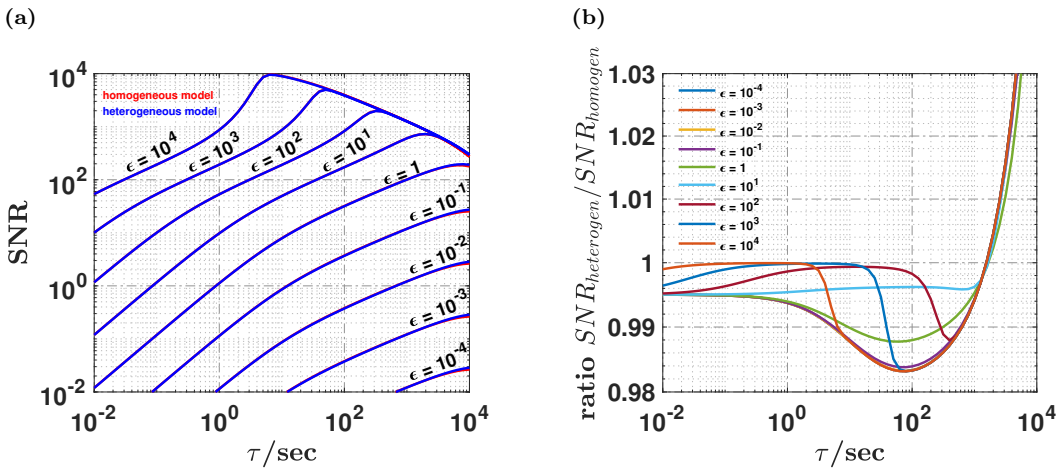

Figure 7 – **SNR models comparaison.** The SNR simulation is represented for different fluxes ϕ expressed as a fraction ϵ of the dark current Id for both the heterogeneous and homogeneous model ((a)). The ratio between the SNR for the heterogeneous and homogeneous model is presented in figure (b).

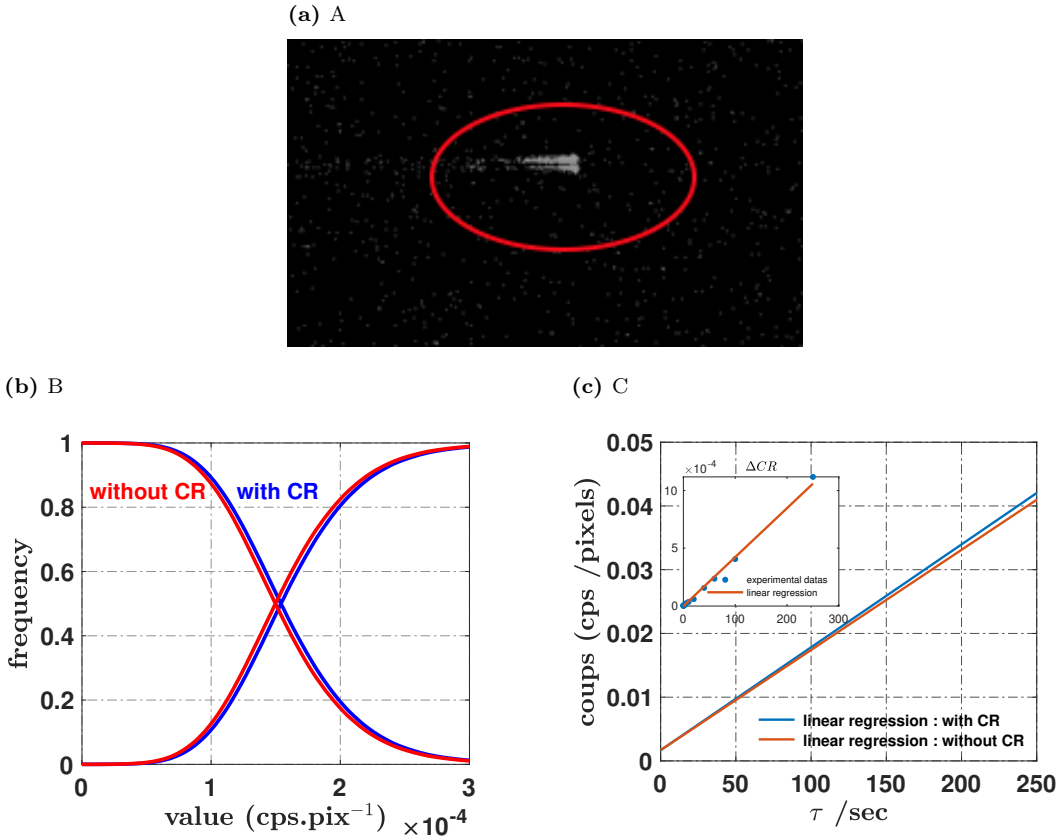

Figure 8 – **Cosmic Rays Frequency**. Aspect of a CR in a frame (a). The cumulative distributive function (CDF) and its complement of the frequency of counts (b), and the linear regression of the number of counts as a function of time is shown before and after removal of cosmic rays (CR) **??**. The experimental difference of the number of counts as a function of time before and after the removal of CR and its linear regression is on the insert of the figure (c).

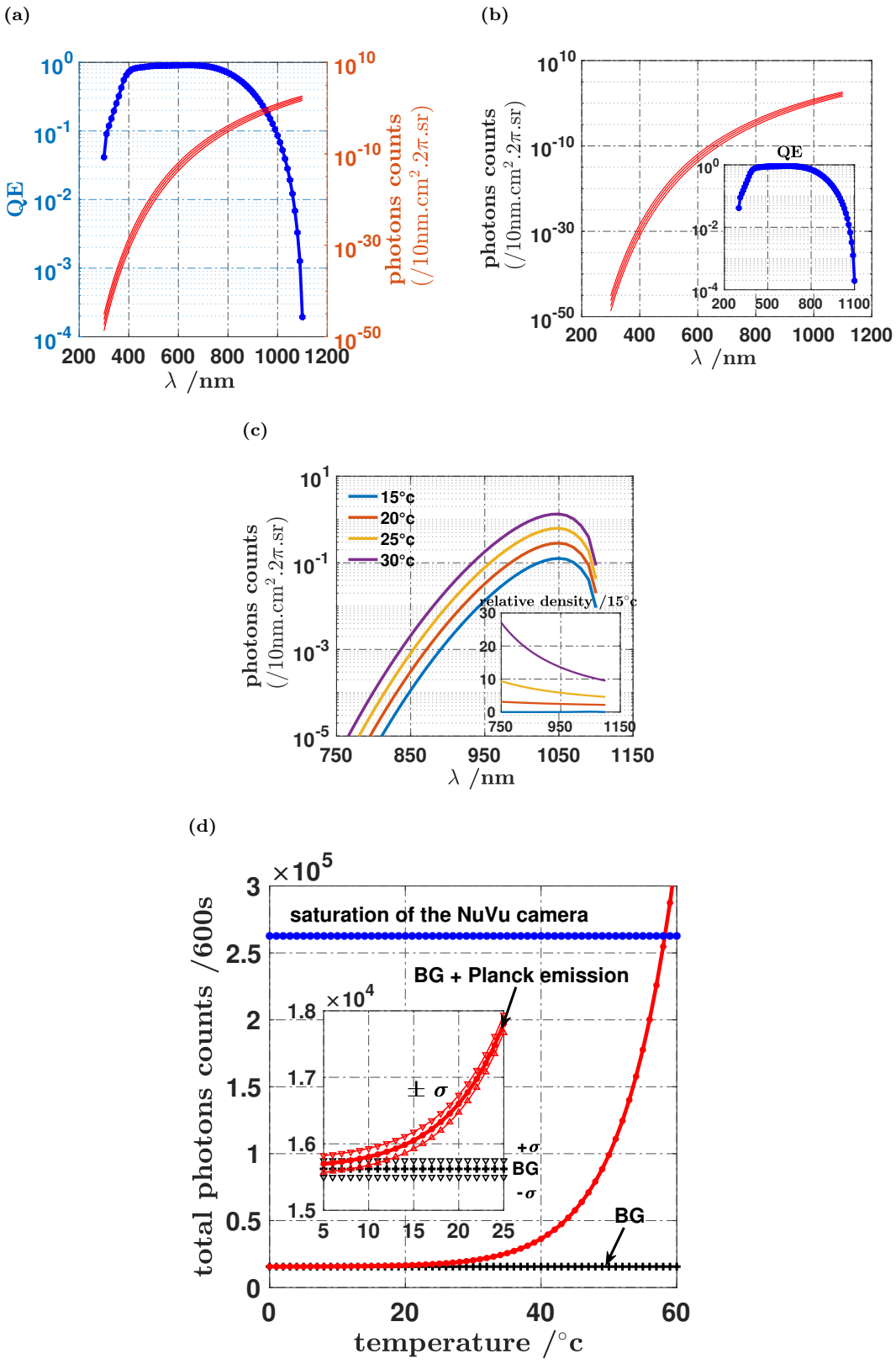

Figure 9 – **Black Body radiation spectra and spectral density of thermal radiation**. The BBR is presented for increasing temperatures of 15, 20, 25 and 30 celsius degrees integrated over 10nm of wavelength during 1 second for 1 cm^2 surface over 2π sr. The inserted figure shows a zoom over $\lambda = [0.7 - 1.1]$ nm, representing the spectral density relative to 15^{o}c ((c).) **Quantum Efficiency of the Nuvu Camera and spectral density of thermal radiation**. Y axe is in logarithmic scale to show the dramatic decrease of the detectability when going toward shorter wavelength, the quantum efficiency of the NüVü camera is represented along with the spectral density of the thermal radiation. ((a) and (b).) **Model : NuVu Camera counts (N1) as a function of the temperature** . The N1 is given by summing the BackGround (BG) noise of the NuVu camera and the detected flux of the BBR. This detected flux is found by integrating the BBR over the QE as a function of λ for a $\tau = 600s$. The pixels saturation level is shown ($N1 = \sum_{ij} pixels$). The inclusion shows the temperatures for which the detected Planck flux emission begins to be significantly detectable ((d).)

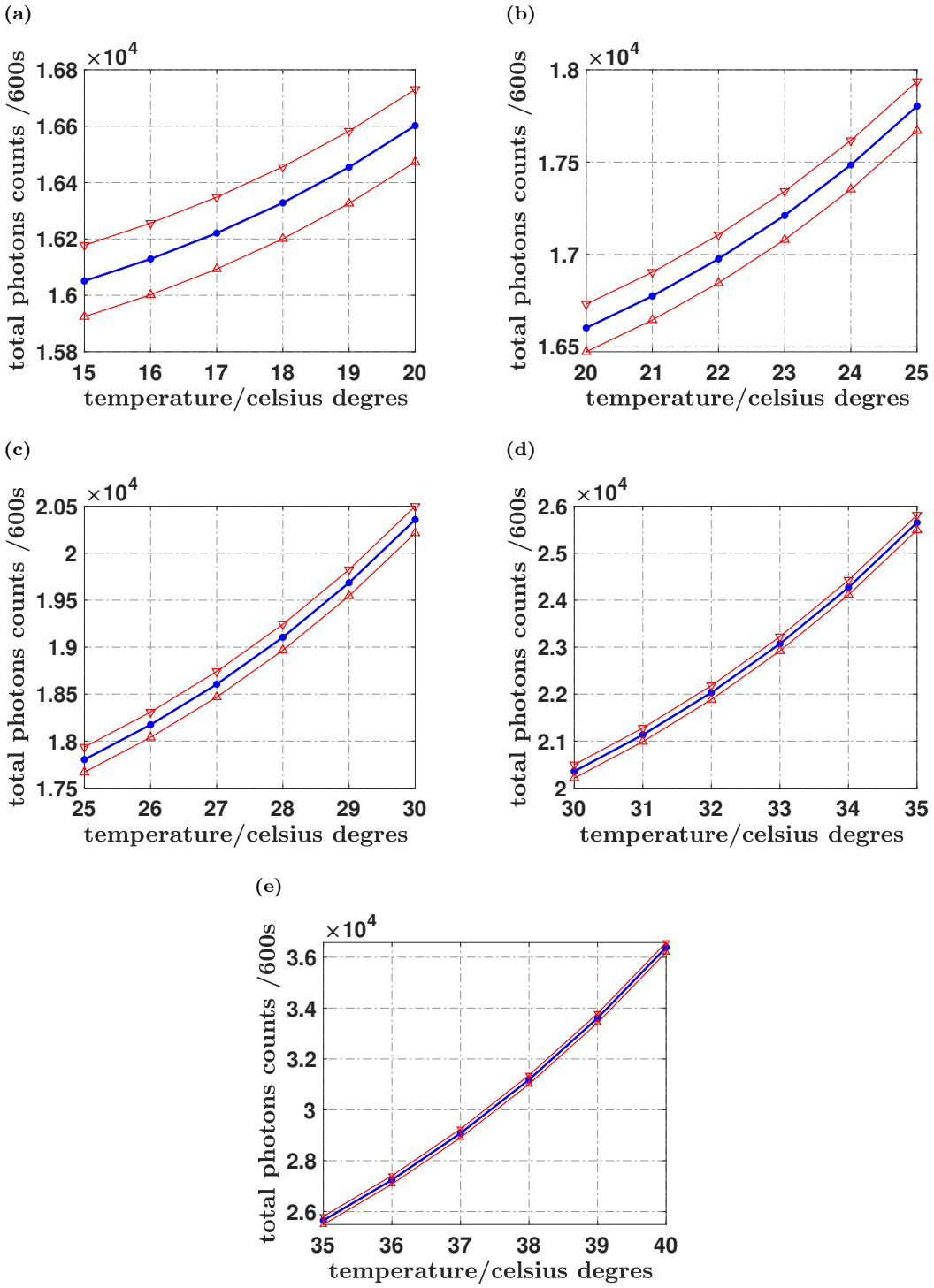

Figure 10 – **NuVu Camera counts (N1) as a function of the temperature : zoom**. Here is shown how the Noise Equivalent Temperature Difference (NETD) decrease dramatically with the increasing of the temperature. Arrows are showing the standard deviation of the measure according to the model. (A), (B), (C), (D), (E) from [15 to 20], [20 to 25], [25 to 30], [30 to 35], [35 to 40] celsius degrees respectively.

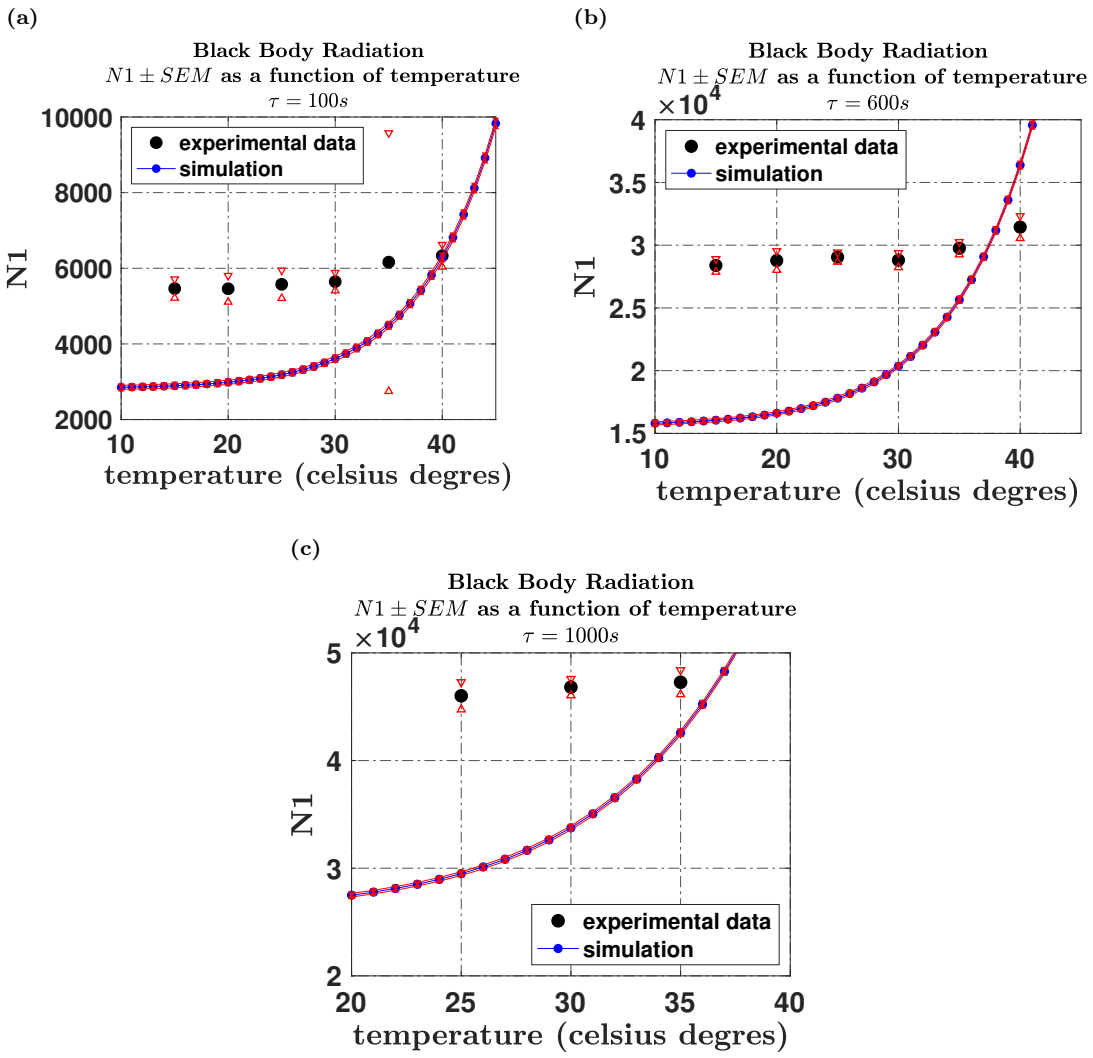

Figure 11 – **Black Body radiation detection**. The BBR is directly measured for increasing temperatures with different times of exposures (100 s ((a)), 600 s ((b)), 1000 s ((a))), and compared to the simulation (9.)

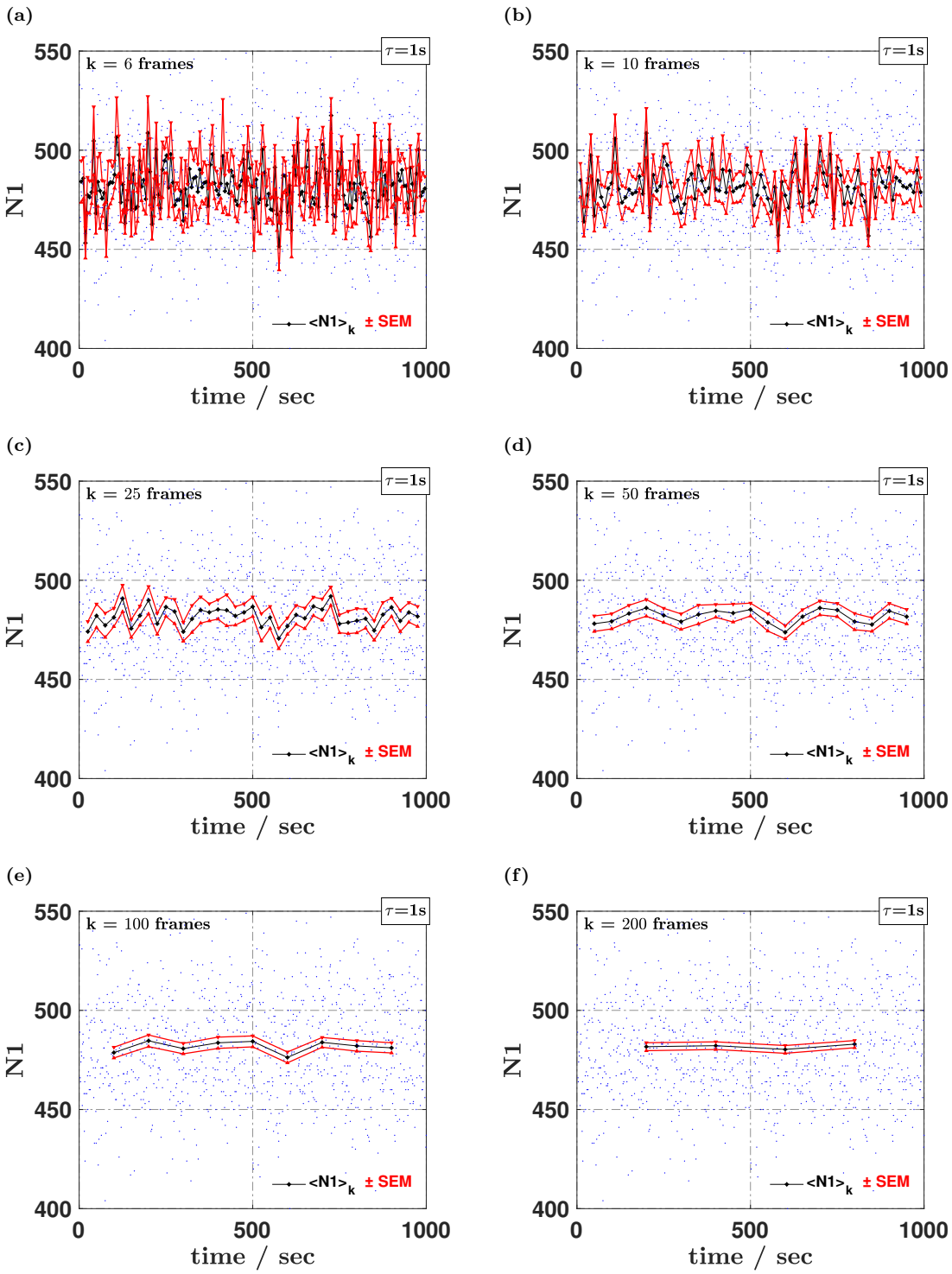

Figure 12 – **Stochastic Filter (τ = 1s)** . During background camera measurement, moving average of the total counts on the sensor ($< N1 >_k$) for k data points (N1, blue dots) and its standard deviation of the mean (SEM) during τ =1second. Increasing k shows that significative fluctuations are detectable during time while increasing the period until 200 seconds for a τ = 1s (f).

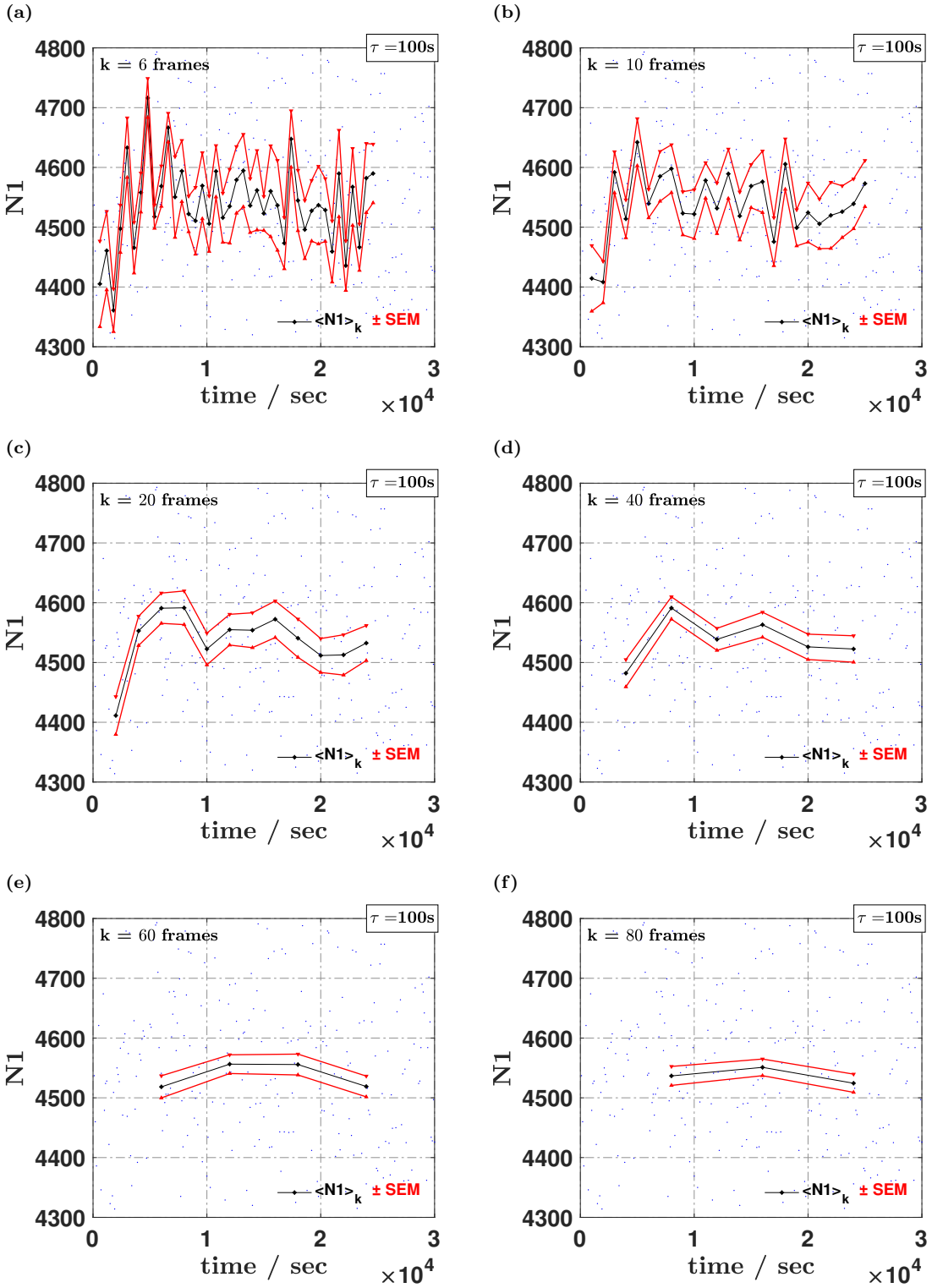

Figure 13 – **Stochastic Filter (τ = 100s)** . During background camera measurement, moving average of the total counts on the sensor ($< N1 >_k$) for k data points (N1, blue dots) and its standard deviation of the mean (SEM) during τ =100second. Increasing k shows that significative fluctuations are detectable during time while increasing the period until 8000 seconds for a τ = 100s (f).

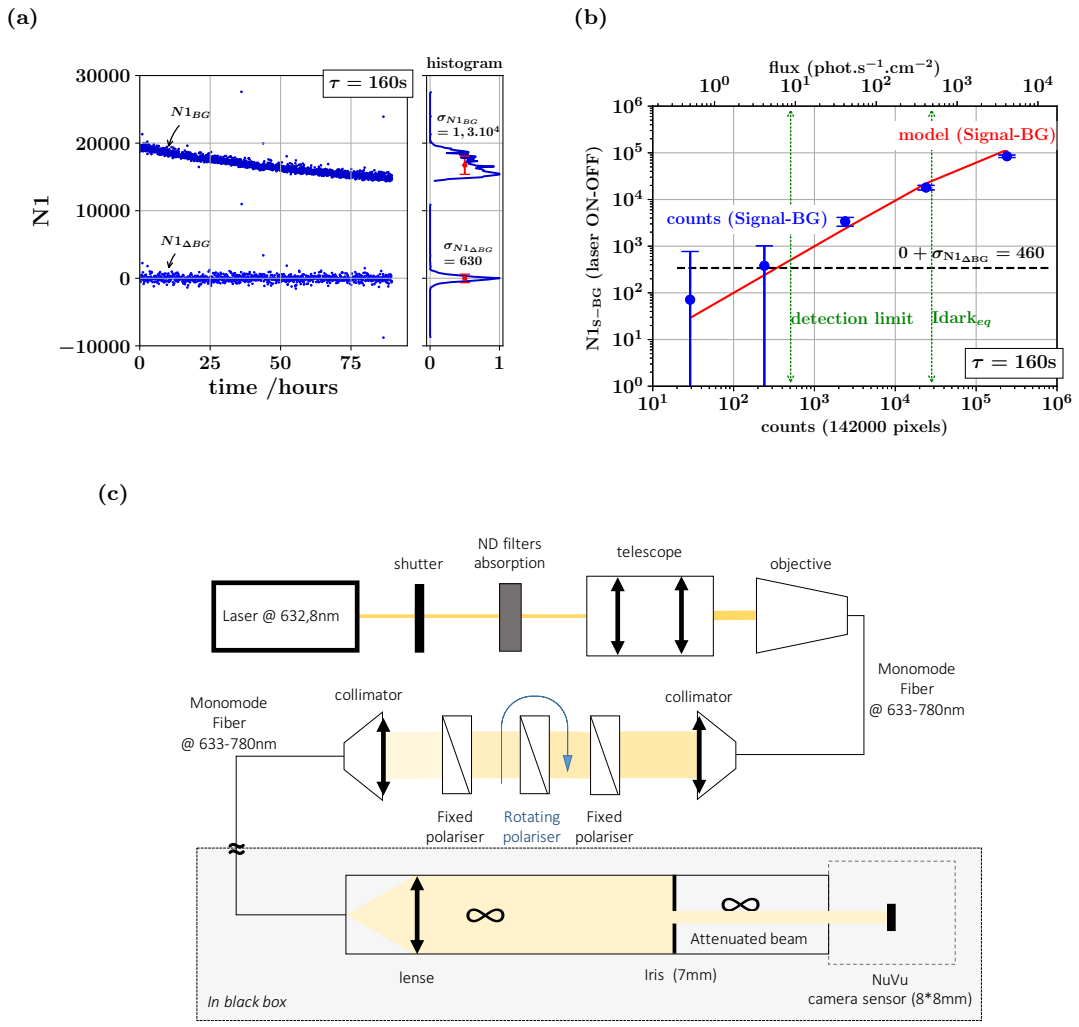

Figure 14 – **Experimental calibration and noise subtraction to free measurement from low frequencies noise variations**. (a) : Raw data taken in the most possible darkness on the entire surface sensor, (ie shutter closed), ($N1_{BG}$) show a slow relaxation process. When subtracting neighbouring data points ($N1_{\Delta BG}$), the observed variance is lower than the expected variance for non correlated measurements, and only high frequency fluctuation from the camera sensor noise remains (variation between two neighbouring points.) The distribution of both set of data point is respectively shown by the histograms. (b) : Calibrated flux detection with the NuVu camera and comparaison of the experimental results and the model describing the behavior of the NuVu camera. The datas are the average of the difference between the average photons counts inside the area illuminated by the laser beam (40 mm diameter disk) during the time of exposure of optimal density (160sec), and the environmental noise (determined with the shutter open while the LASER is off). All statistics are made on the difference between the signal (camera shutter open) and the camera noise (camera shutter closed : BG). The limit of detection (black dotted line) is the noise fluctuations at higher relative frequencies (points near in time). For approximately 142000 pixels (illuminated area on the detector), this limit is 460 counts for 160sec. The green dotted lines shows the equivalent light flux corresponding to that detection limit (8.8ph.s^{-1}.cm^{-2}) in those conditions, and the dark current equivalent flux (Idark$_{equ}$ = 485 ph.s^{-1}.cm^{-2}). (c) : Experimental setup to produce a beam of calibrated low light fluxes. The final optical elements are placed in a thorlab SM1 tube and fixed on the camera via c-mount. We only select the central zone of the infinite attenuated beam to have a better average flux uniformity throughout the beam section.